1,4

A Direct Micromechanical Approach toward the Development of Quadratic Stress Gradient Failure Criteria for Textile Composites

RYAN L. KARKKAINEN[†] AND BHAVANI V. SANKAR*,[‡]
Department of Mechanical & Aerospace Engineering, PO Box 116250
University of Florida, Gainesville, FL, 32611-6250, USA

JEROME T. TZENG[§]
US Army Research Laboratory, Aberdeen Proving Ground, MD 21005-5066, USA

(Received Febrary 14, 2006)
(Accepted July 12, 2006)

ABSTRACT: Based upon previous results of direct micromechanical method (DMM) analysis of the representative volume element (RVE) of a plain-weave textile composite, two methods for predicting failure envelopes are presented: a parametric ellipse-fitting scheme and a 27-term quadratic stress-gradient failure criterion. Both include the consideration of micro level stress gradients and effectively predict failure in agreement with the DMM. The parametric ellipse-fitting method was found to agree with DMM results to within a few percent. The quadratic failure criterion was found to agree within 9.3%, but the method is more robust in its ability to predict failure for complex loading cases.

KEY WORDS: textile composites, strength, finite element analysis.

INTRODUCTION

DESIGNS OF CURRENT textile composite structures are often based upon well-known phenomenological failure criterion. Although micromechanical models have been successfully employed in predicting thermo-elastic constants of fiber-reinforced composite materials, their use for strength prediction in multiaxial loading conditions is not practical, as computational analysis must be performed for each loading case. The development

*Author to whom correspondence should be addressed. E-mail: sankar@ufl.edu
[†]Graduate student (rkarkkai@ufl.edu), currently with Army Research Laboratory, Aberdeen, MD, USA.
[‡]Newton C. Ebaugh Professor.
[§]Research engineer.
Figures 1, 3 and 6–10 appear in color online: http://jcm.sagepub.com

0021-9983/0?/00 0001–21 $10.00/0 DOI: 10.1177/00219983O?069905

of commonly employed failure theories has generally been based upon the mechanical behavior of unidirectional composite materials. However, woven or braided textile composites present increased microstructural complexity and unique challenges as compared to a unidirectional composite. Laminate analysis, property homogenization, and other common approaches will no longer apply. Thus, current designs of textile structures will not be optimized for maximum damage resistance and minimum weight. The employment of textile composites requires unique approaches to micromechanical analysis, the results of which can be incorporated into an appropriate failure theory.

Phenomenological failure criteria are still the predominant choice for design in industry. There are three major types of engineering failure criteria for unidirectional composite materials: maximum stress criterion, maximum strain criterion, and quadratic interaction criterion, such as the Tsai–Hill and Tsai–Wu failure theories [1]. Towards development of new failure theories, most of the micromechanical modeling work done thus far have focused on predicting thermo-mechanical properties. Most of the current analytical and numerical methodologies developed to characterize textile composites assume that the textile composite is a homogeneous material at the macroscopic scale.

A more detailed survey of current research in the area of failure modeling of textile composites is offered in a companion study [2] to the current paper. A sampling of these works is presented below for clarity and ease of reference.

Initial and progressive failure of a plain weave composite [3] using finite element analysis has provided insight into the failure modes under axial loading conditions. The capability for more detailed stress fields in the representative volume element (RVE) under investigation has been included [4], and techniques have been developed to minimize required computation times [5]. Accurate stress distributions for plain weave composites in flexure have been investigated, and effective stiffness properties for multi-layer specimens have been predicted [6].

The binary model [7,8] utilizes 1-D line elements to represent fiber tow embedded within the bulk matrix. This allows for quick and efficient finite element analysis of any textile weave of interest, and is robust for alteration of micro-architectural parameters such as tow waviness, tow misalignment, varying weave architectures, etc. Some micro-level stress field detail is lost while still maintaining accurate macro-level representation.

The analytical method referred to as the mosaic model and its adaptations [9,10] represent a textile composite RVE as an assemblage of homogenized blocks, each with unidirectional composite or matrix properties. Classical laminated plate theory can be used to determine the global stiffness matrix of the RVE. For macroscopically homogeneous load cases, good agreement has been shown with experimental data.

Effective prediction of compressive strength of braided textile composites using a detailed finite element method (FEM) micromechanical model has been performed [11], which shows good comparison to experimental results in a parallel study [12]. Biaxial loading is considered in both the experimental and computational analyses. Buckling analysis has been performed, and the effects of tow waviness and micro-architecture on the compressive strength are shown.

Modeling of damage initiation and progression utilizing finite element methods and new methods to replace traditional property knockdown schemes after element-failure have been accomplished for general composite structures [13]. This utilizes a relatively new failure criterion [14] which in itself has been used to effectively predict damage in composite materials by analysis of the strain state including dilatational induced damage initiation.

A previous study by the authors [2] extended a method, known as the direct micromechanics method [15] (DMM), to develop failure envelopes for a plain-weave textile composite under plane stress in terms of applied macroscopic stresses. The micro-scale stresses within the RVE were computed using finite element methods. The relation between the average macrostresses and macro-strains provide the constitutive relations for the idealized homogeneous material. The micro-stresses are used to predict the failure of the yarn or matrix, which in turn translates to failure of the textile composite.

The current paper presents methods based upon the results of a previous study [2] to develop a failure criterion for textile composites. The methodology herein can then be extended in general to any textile composite of interest. Using the DMM, the failure envelope is developed for in-plane force resultants, with and without moment resultants. No currently accepted failure criteria exist that may be used explicitly for the analysis of textile composites, or which include this ability to account for stress gradients at the micromechanical level. Thus the methods and results employed herein are used to develop phenomenological failure criteria for textile composites. Based on the DMM results, two methods are presented which may be used to predict failure of a textile composite. The first is a parametric method based on prediction of regular trends in the failure envelopes of a given 3D stress space. The second method represents the formulation of a 27-term quadratic failure equation that can be evaluated to determine failure of the textile under any general force and moment resultants.

METHODS

Finite Element Micromechanical Method

Micromechanical analysis has been performed to determine the stiffness, strength, and failure envelopes of a plain weave textile composite. Details of this analysis are available in a previous study [2], but methods therein are presented here in an abbreviated fashion. In the previous study, stress gradient effects are investigated, and it is assumed that the stress state is not uniform across the RVE. This represents an extension of the micromechanical models used to predict the strength of textile composites [15–18]. The stress state is defined in terms of the well-known laminate theory force and moment resultants, $[N]$ and $[M]$, in which the latter term captures the presence of a stress distribution or gradient that is typically neglected. Furthermore, structural stiffness coefficients analogous to the $[A]$, $[B]$, $[D]$ matrices are defined. In this approach, these structural stiffness coefficients are computed directly from the micromechanical models, rather than making conventional approximations. Thus, in the current paper, failure envelopes and stress analysis are described in such terms. Some of the basic assumptions of micromechanics will still apply to the current work. For example, it is assumed that the RVE is truly representative at the macro level. Further, as will be shown more clearly in discussion of the DMM for failure analysis, it is assumed that the micro level (element level) failure criteria is known. Also, the criteria developed later in this paper apply to plane stress states. For thick composites which may show appreciable through thickness stresses, extra analyses extending the current methods must be performed.

The textile architecture under investigation is a plain weave, and this RVE is shown in Figure 1. This architecture was chosen from a literature source [19] that provided a complete and detailed description of the needed geometrical parameters.

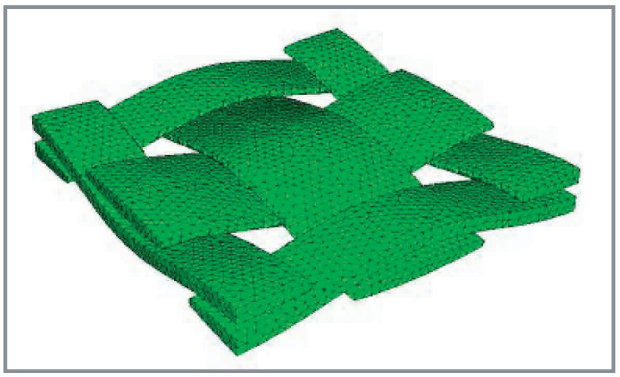

Figure 1. *RVE geometry of a plain weave textile composite.*

Given parameters are representative of micro-architectures as experimentally observed via SEM or standard microscope. Total fiber volume fraction, given these dimensions, will be 25%, incorporating the fact that the resin-impregnated tow itself has a fiber volume fraction of 65% (this is calculated directly from the finite element software ABAQUS™ which yields element volumes as outputs, thus the volume of all matrix elements can be compared to the volume of all tow elements). Though this volume fraction may seem low for structural uses, it can be representative of many significant low-load, impact-resistant applications, such as automotive lightweight body panels. It should be noted that a number of parameters such as tow spacing, tow dimensions, shape of tow cross section, RVE dimensions, etc., are required to exactly specify the textile geometry. These specifications will have a significant effect on micromechanical modeling. Consequently, care should be taken when comparing the results to ensure that textile geometries under comparison are equivalent.

In order to evaluate the stiffness and strength properties of the textile composite under consideration, the DMM is essentially employed as an analytical 'laboratory' that quickly and effectively simulates physical testing and experimental procedures. Though experimental verification remains a baseline of veracity to FEM analysis, once such checks have been performed this procedure effectively overcomes the limitations of physical apparatus and can rapidly populate diverse failure spaces. Also, results achieved from the DMM are completely three-dimensional stress or strain fields, i.e., the results can be visualized throughout the thickness of the specimen. This overcomes the limitations inherent to physical application of experimental stress analysis techniques, which are labor-intensive and generally limited to surface visualizations.

In the direct micromechanics method (DMM), the RVE is subjected to macroscopic force and moment resultants, which are related to macroscopic strain and curvature according to:

$$\begin{Bmatrix} \{N\} \\ \{M\} \end{Bmatrix} = \begin{bmatrix} [A] & [B] \\ [B] & [D] \end{bmatrix} \begin{Bmatrix} \{\varepsilon\} \\ \{\kappa\} \end{Bmatrix} \tag{1}$$

Thus the constitutive matrices must be evaluated to determine this correlation. Note that Equation (1) borrows the nomenclature of classical laminate theory but does not represent a direct employment of this theory. This is to say that such nomenclature is used to incorporate the consideration of micro level stress gradients as mathematically accounted for by inclusion of moment resultant terms (M_{ij}). Once this relationship has been determined, a macroscopic deformation can be applied using an FEM code.

In this way, the FEM results for stress in each element yield the microstresses resulting from an applied force or moment resultant.

The RVE is subjected to independent macroscopic unit deformations in order to fully evaluate the stiffness matrices of Equation (1). In each of the six cases, a single unit strain or a single unit curvature is applied, and all other deformation terms are set to zero, and the appropriate periodic boundary conditions are applied [2,14].

The FEM results for each element yield the microstresses resulting from a given macro-level strain and curvature. The corresponding macro-level force and moment resultants in each case can be computed by averaging the microstresses over the entire volume of the RVE:

$$N_{ij} = \left(\frac{1}{\mathrm{ab}}\right) \sum_e \sigma_{ij}^e V^e \tag{2}$$

$$M_{ij} = \left(\frac{1}{\mathrm{ab}}\right) \sum_e z\sigma_{ij}^e V^e \tag{3}$$

where e denotes summation over all elements in the FE model of the RVE, V^e is the volume of the eth element, and a and b are the dimensions of the RVE as shown in Figure 1. These equations determine the overall macro level force and moment resultants, which are calculated as the net effect of the microstress field throughout the volume of the RVE as taken from the FEM results. The volume averaging accounts for the fact that smaller elements represent a smaller contribution to the total macro level force or moment resultant, and vice versa.

Thus the constitutive matrices of Equation (1) can be found by independently evaluating six unit strain and curvature cases, in tandem with Equations (2) and (3). By applying the appropriate displacements which correspond to a given unit strain or curvature case, the stiffness coefficients in a column corresponding to the non-zero strain can be evaluated directly from the force and moment resultant values as calculated from the finite element micro stresses via Equations (2) and (3). Thus the six load cases completely describe the six columns of the $[A]$, $[B]$, $[D]$ matrix. Again, the reader is referred to our previous work [2] for more details on these methods.

Direct Micromechanics Method for Failure Analysis

The method described above can be used to predict failure strength by comparing the computed microstresses in each element against failure criteria for the constituent yarn and matrix of the textile composite. The microstresses in each element can be extrapolated from the preliminary RVE analysis (described above) of each of the six linearly independent macrostrain components. The microstress state for a general applied force or moment resultant is obtained by superposing multiples of the results from the unit macrostrain analysis:

$$\{\sigma^e\} = [F^e] \begin{Bmatrix} \varepsilon^M \\ \kappa^M \end{Bmatrix} \tag{4}$$

where the 6×6 matrix $[F^e]$ contains the microstress in element e resulting from the unit strain and curvature analysis. For example, the microstress σ_y in the RVE for $\varepsilon_{x0} = 0.05$ and $\kappa_y = 0.003\,\mathrm{m}^{-1}$ is calculated as $\sigma_y = 0.05F_{21} + 0.003F_{25}$.

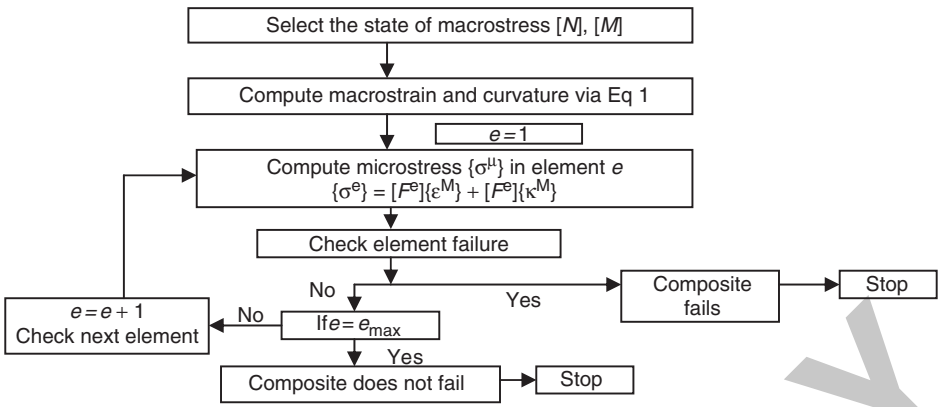

Figure 2. *Flowchart for failure analysis using the direct micromechanics method.*

Failure is checked on an element-by-element basis, and the failure criterion of each element can be selected appropriately based upon whether it is a yarn or matrix element. It is assumed that the entire textile composite has failed, even if only one of the yarn or matrix elements has failed. Although this may be considered conservative, it is realistically representative of the initial failure of the composite. It can be thought of by analogy to the first-ply failure of a laminated composite, i.e., the point at which property loss becomes significant, even if remaining material can continue to support applied loading. For the isotropic matrix elements, the maximum principal stress criterion is used to evaluate element failure. For fiber tow elements, the Tsai–Wu failure criterion is used. This criterion is more suitable to the orthotropic nature of the fiber tow, which is essentially a unidirectional composite at the micro level. Microstresses in the yarn are transformed to local coordinates tangent to the path of the yarn and compared to strength coefficients for a unidirectional composite, using the Tsai–Wu criterion.

A flow chart that describes the DMM procedure is shown in Figure 2. Failure envelopes are generated by first selecting a macrostress state to investigate. Then the macrostrains and curvatures resulting from this applied loading are calculated from Equation (1). The resulting stress field for the entire RVE is then calculated by Equation (4), based on the scaled superposition of the results from FEM analysis of the unit load cases. Failure is then checked in each element against a given failure criterion. This cycle is then repeated while progressively increasing a selected force or moment resultant, and holding all others constant until an element level failure criterion is exceeded. If a particular failure criterion is exceeded, the element and the RVE are considered to have failed, which then defines the threshold of the failure envelope at a given point. Thus failure envelopes for the textile composite can be generated in various force and moment resultant spaces.

RESULTS

A Parametric Approach to Predicting Failure Envelopes for a Given 3D Stress Space

Based on an extension of the results presented in more detail in [2] and shown here in Figure 3, failure envelopes in the space of N_x–N_y–M_x (a practical and useful failure space which illustrates the limits of biaxial loading and the importance of consideration

of stress gradients across an RVE) were seen to be characteristically elliptical in nature. This is due to the prevalence of stress interaction effects, as well as the symmetry of the plain weave geometry under analysis.

Figure 3 shows the discrete failure points as determined from the DMM for cases of biaxial loading with constant applied moments of 0, 0.3, 0.5, and 0.8 times the critical moment that would cause failure if it were the only load present. Also shown in this figure are elliptical fits to each failure envelope, which were computed by a Matlab™ based routine that was used to determine a least squares fit to the DMM data points.

Phenomenologically, it can be seen that the failure envelopes become smaller as a larger moment (stress gradient) is applied. An applied moment has the expectable effect of shrinking the failure envelope, though in limited regions it has been seen that the complexity of the superposed stress fields may have an offsetting or beneficial effect.

Analytically, it can be seen that there are definite trends in the axes and placement of the failure ellipses. Failure ellipses were characterized with parameters such as major axis length, minor axis length, ellipse axis orientation angle, and the ellipse center point. Any general ellipse in (x, y) space can be represented by the expression:

$$\left[\frac{x\cos\theta + y\sin\theta - u_0}{a}\right]^2 + \left[\frac{-x\sin\theta + y\cos\theta - v_0}{b}\right]^2 = 1 \tag{5}$$

where θ is the orientation angle of the major axis of the ellipse with respect to the x-axis, u_0 and v_0 are the coordinates of the ellipse center point, a is half the major axis length, and b is half the minor axis length. For each failure ellipse shown in Figure 3, these parameters were then plotted as functions of the moment applied for each case, in order to inspect parametric trends.

For example, Figures 4 and 5 show the major and minor axis length of several $N_x - N_y - M_x$ failure envelopes plotted against the moment resultant M_x applied in each case. A limited number of fitting cases were used, in order to reserve an adequate number of test cases and to prevent over-fitting of the trends. As mentioned earlier and as seen in the figures, a larger applied moment with a given failure envelope has the effect of shrinking the envelope's major and minor axes. These trends were regular enough to be closely approximated with a polynomial trend line. For an applied moment equal to the critical moment (the moment resultant which would cause failure if it were the only load present), the ellipse axes lengths become zero, as a load sufficient for failure is already applied, and no additional force resultants may be applied.

In addition to shrinking the failure envelope, larger applied moments also tend to cause a small but significant shift in the center point of the failure ellipse. This is caused by the fact that an applied moment is still a directional loading, and thus produces a directional bias in the location of the failure envelope. These trends were also plotted (Figure 6) and approximated with polynomial trend lines. Ellipse orientation angle (θ) was found to be very nearly constant, regardless of loading conditions, and thus no trend plot is shown.

Based on the above, an elliptical failure envelope of the form of Equation (5) can be predicted by evaluating the expressions for ellipse parameters in terms of applied moment resultant, as shown below:

$$\left[\frac{N_x\cos\theta + N_y\sin\theta - u_0}{a}\right]^2 + \left[\frac{-N_x\sin\theta + N_y\cos\theta - v_0}{b}\right]^2 = 1 \tag{6a}$$

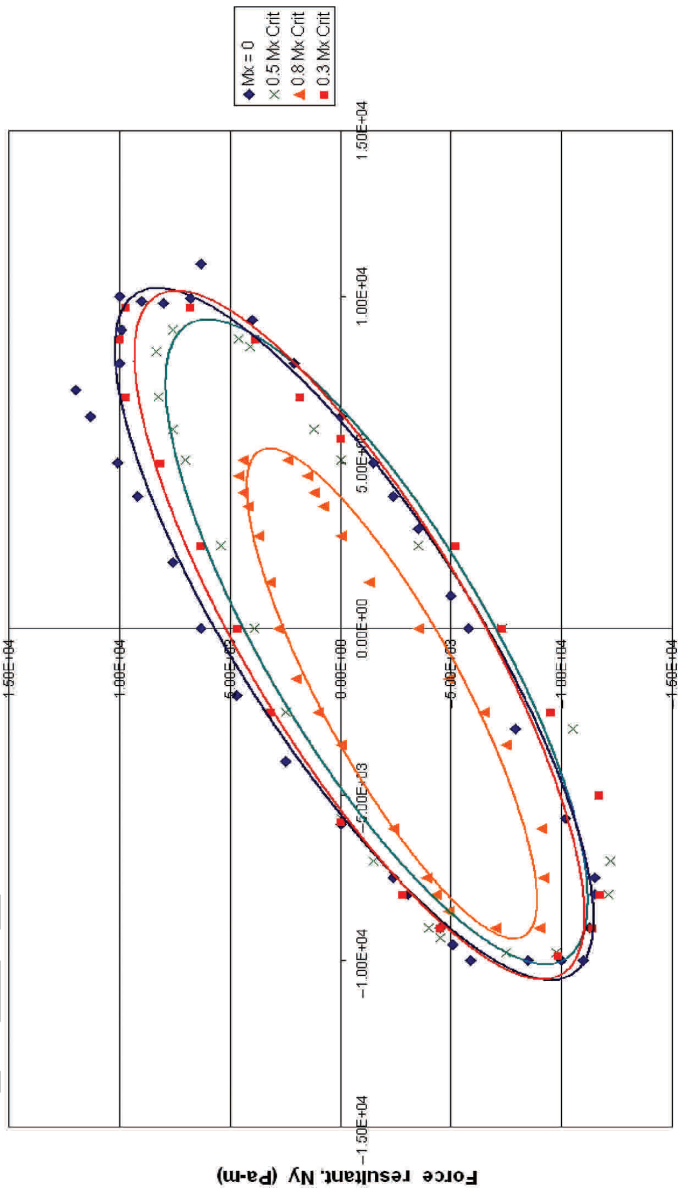

Figure 3. *DMM failure envelopes for biaxial loading with multiple constant applied moments. An ellipse is fit to each data set using a least-squares method.*

+ [Ver: 8.07r g/W] [30.8.2006-6:49pm] [1-22] [Page No. 8] FIRST PROOFS K:/Journals/Inprocess/Sage/Jcm/JCM 069905.3d (JCM) Paper: JCM 069905 Keyword

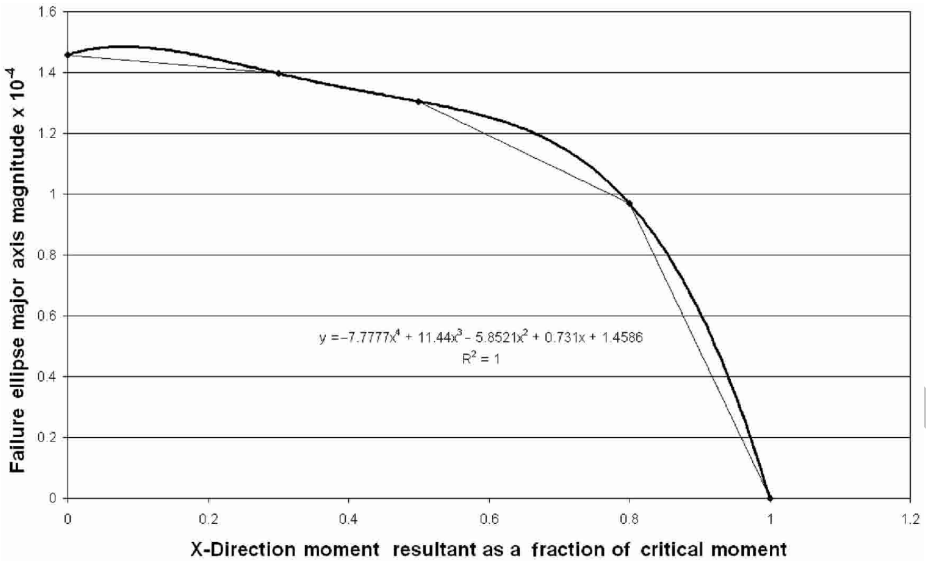

Figure 4. *Effect of applied moment resultant on the major axis of elliptical failure envelopes.*

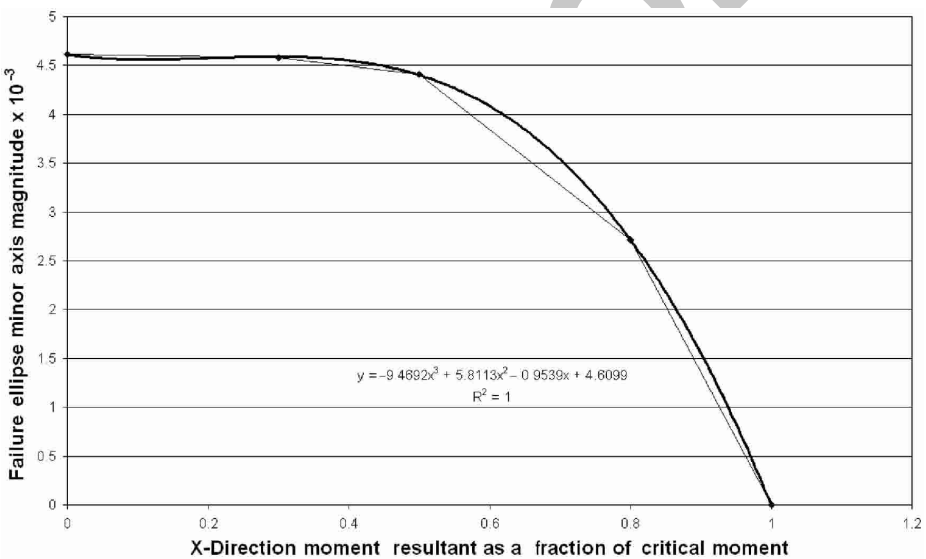

Figure 5. *Effect of applied moment resultant on the minor axis of elliptical failure envelopes.*

$$
\begin{aligned}
M &= \frac{M_{\text{applied}}}{M_{\text{critical}}} \\
a &= -7.77M^4 + 11.44M^3 - 5.85M^2 + 0.73M + 1.4586 \\
b &= -9.47M^3 + 5.81M^2 - 0.95M + 4.6 \\
u_0 &= -3.48M^2 - 0.51M \\
v_0 &= 3.26M^2 - 5.92M
\end{aligned}
\tag{6b}
$$

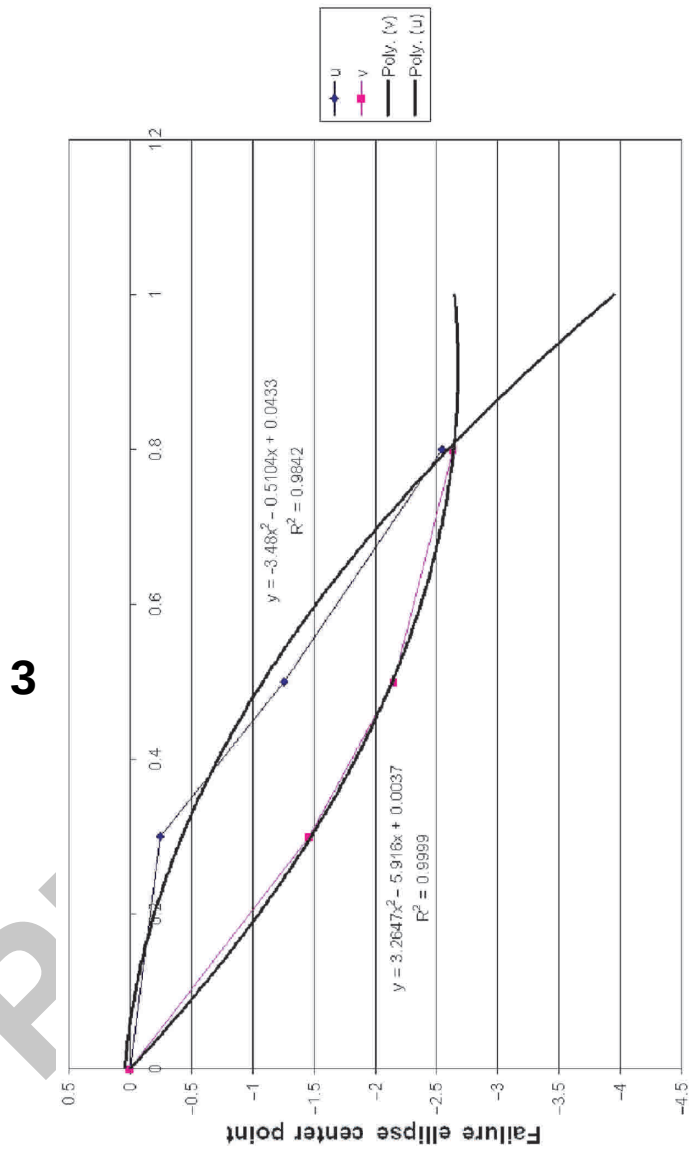

Figure 6. *Effect of applied moment resultant on the center point coordinates (u_o, v_o) of elliptical failure envelopes.*

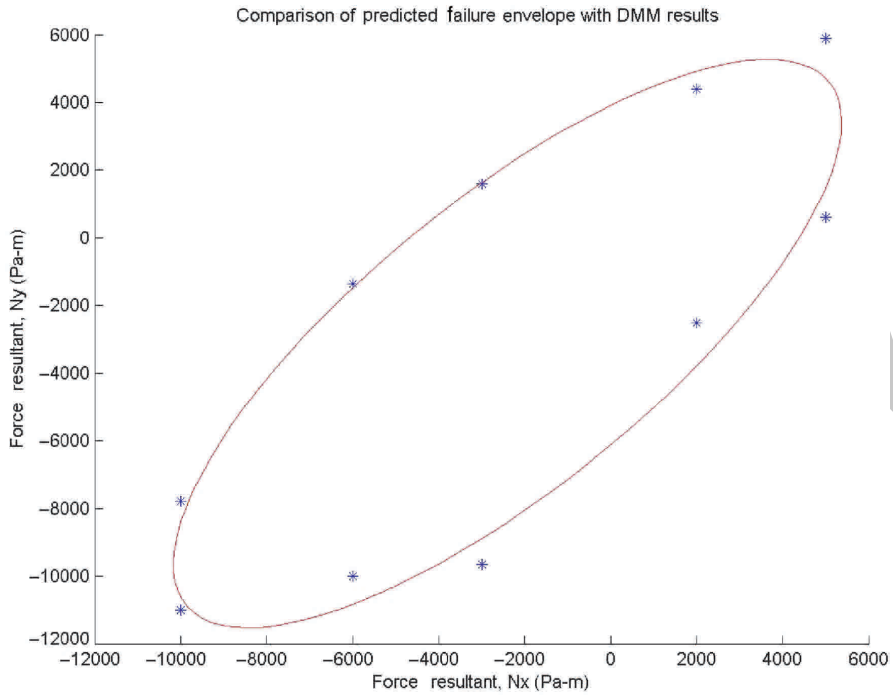

Figure 7. *Failure envelopes predicted with the parametric approach as compared to DMM results (applied moment resultant of 0.65 critical moment).*

Thus a failure envelope for the plain-weave textile geometry of Figure 1 with any combination of loads N_x–N_y–M_x can be predicted with the above procedure and by substituting loads into the expression of Equation (6a). For several test cases, a failure ellipse is predicted and compared to discrete failure points as calculated directly from the DMM. These comparisons are shown in Figures 7 and 8. The average deviation between the failure envelopes predicted from the parametric curve fitting as compared with the direct results of micromechanical modeling was less than 2%.

The greatest value of this parametric approach to predicting failure is that it provides good insight into the exact nature of the failure space under consideration. Further, the results are quite accurate and could be useful for design purposes. However, the load cases are limited, and the methods presented here would have to be extended if more than three simultaneous loads were to be applied and analyzed.

Inspection of Failure Envelopes in Additional Stress Spaces

In general, failure envelopes in spaces other than those shown in Figure 3 will not necessarily be elliptical in nature, as has been observed for cases including shear, twist, and multiple moment loading terms. Figures 9 and 10 show failure envelopes in spaces of M_x–M_y–M_{xy} and N_x–M_x–N_{xy} respectively. Discrete points represent the failure envelopes as determined by the DMM. Also shown for each envelope are predicted envelopes labeled QFT as will be explained later in this paper.

Figure 9 isolates the relative effect of moment resultants, or stress gradients, of varying types on the failure envelope, as well as the interaction of multiple moments.

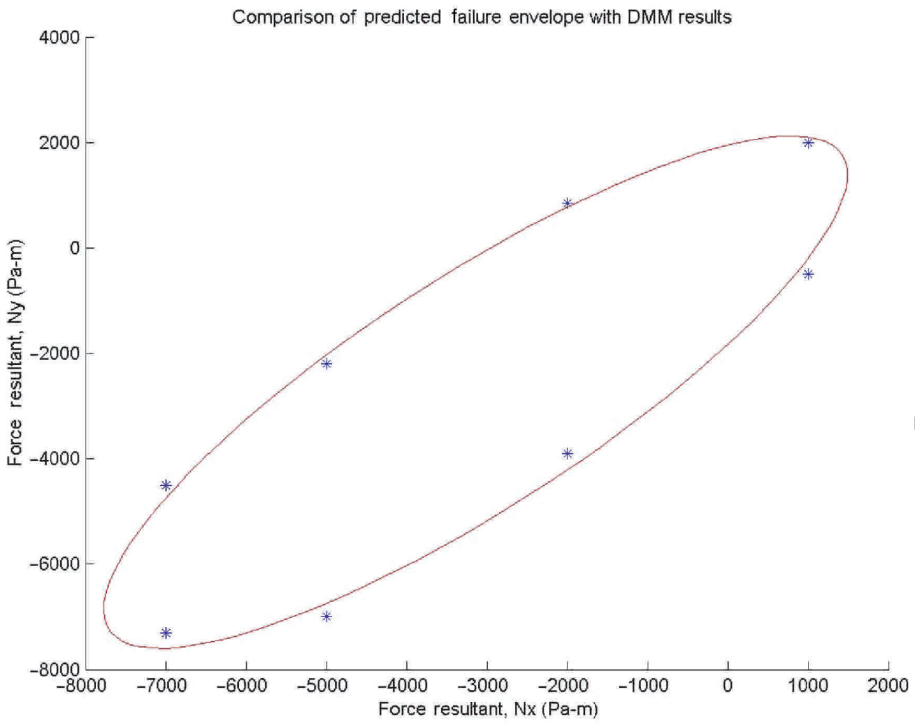

Figure 8. *Failure envelopes predicted with the parametric approach as compared to DMM results (applied moment resultant of 0.9 critical moment).*

Each envelope is mapped out with a constant applied twist M_{xy}. The overall character is in some ways similar to that of Figure 3, i.e., the failure envelope symmetry reflects the symmetry of geometry and loading. Further, the strength limits in quadrants II and IV are lower due to stress interactions. Whereas for biaxial loading, strength is decreased when stresses act in the direction of the natural tendency of Poisson effects, in bending the strength is decreased when biaxial bending acts in the direction of the natural tendency of anticlastic curvature. As is generally seen in all failure analyses that have been performed in this study, the dominant mode of failure is transverse failure of the fiber tow.

The $N_x - M_x - N_{xy}$ failure envelope (Figure 10) provides a visualization of the effect of the magnitude of stress gradient, or loading non-uniformity, for a given force resultant. Each envelope is drawn for constant in-plane shear to further incorporate the effects of multiple loading types. The envelope is symmetric about the x-axis due to the mechanical equality of positive or negative bending moment. This symmetry is not seen about the y-axis since the carbon-epoxy plain weave responds differently in tension or compression.

Development of a Quadratic Stress Gradient Failure Criterion to Predict Failure for 6D Loading

In order to bind together the failure spaces, which can be quite different in nature, as can be seen in Figures 3, 9, and 10, methods of the previous section will not be

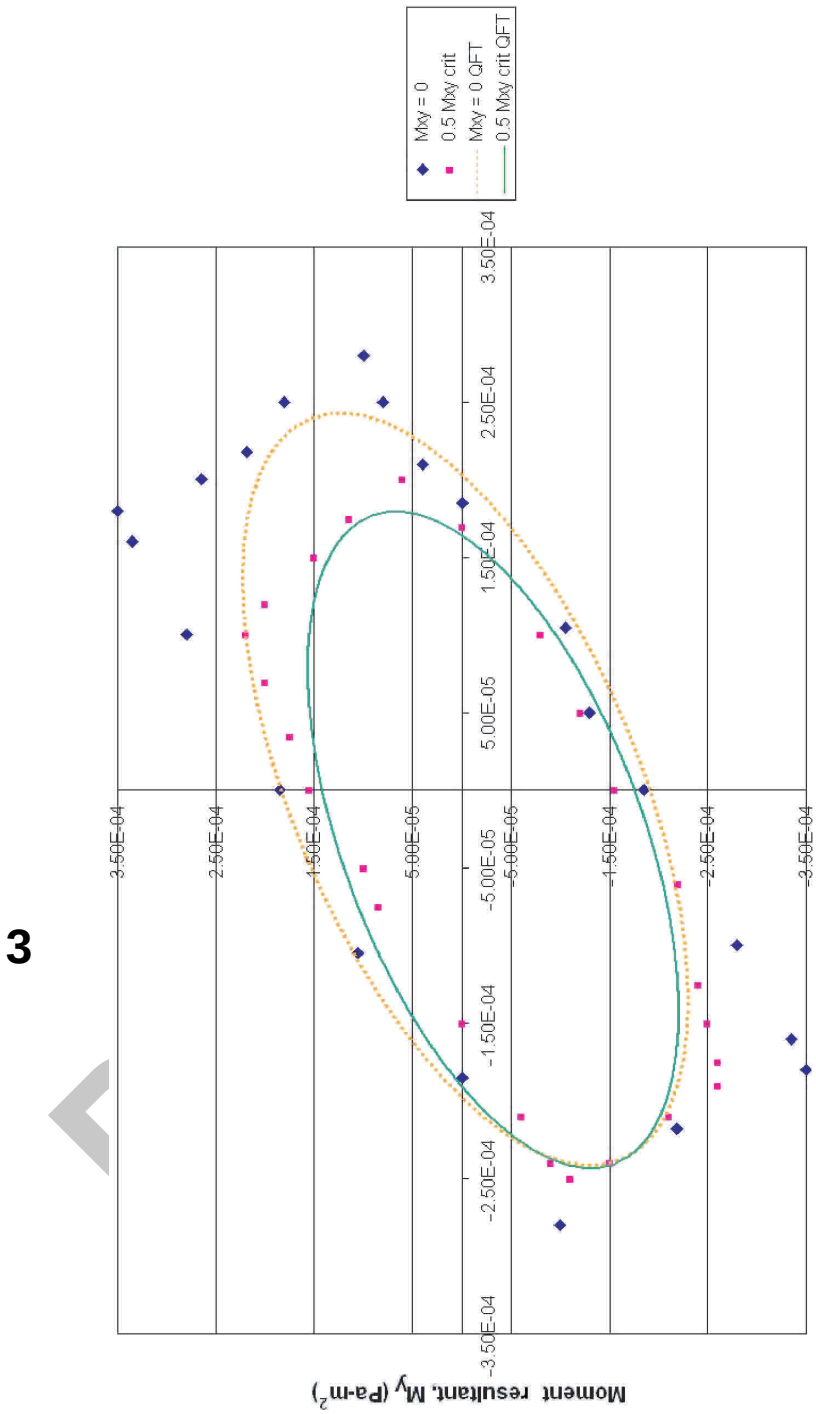

Figure 9. *DMM failure envelopes for biaxial bending with constant applied twisting moment M_{xy}.*

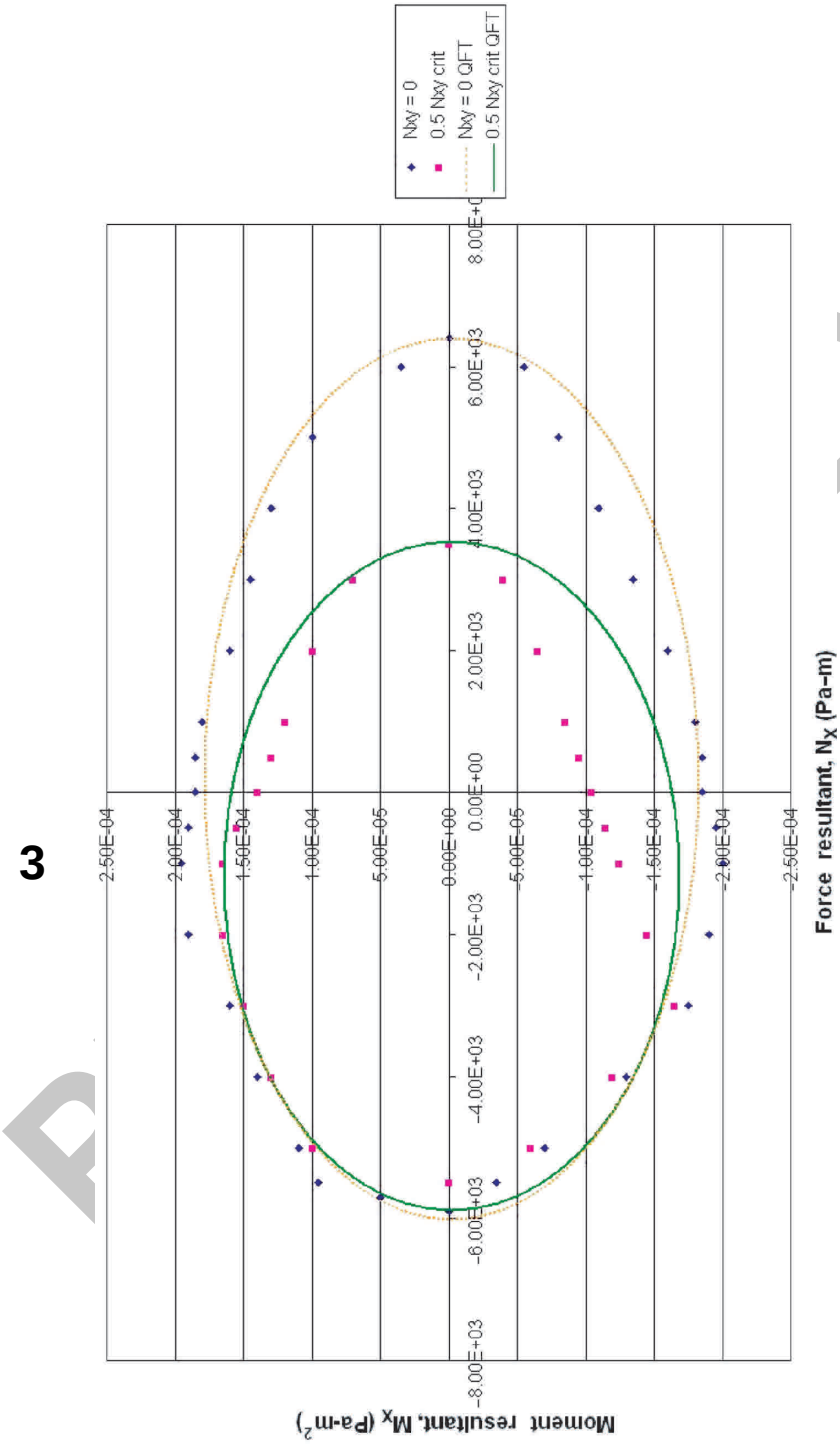

Figure 10. *DMM failure envelopes with force and moment resultants for constant applied in-plane shear N_{xy}.*

readily applicable. Therefore, development of an additional analytical method becomes necessary. Further, an analytical approach to binding the results of multiple failure envelopes as calculated via the DMM, along with the capacity to accommodate any general plate loading condition has a practical value. Given the quadratic interactive nature of the stress state in determination of failure, an expression of the below form has been developed to predict failure:

$$C_{ij}F_iF_j + D_iF_i = 1 \tag{7}$$

where F_i represent general load terms (N_x N_y N_{xy} M_x M_y M_{xy}), and C_{ij} or D_i represent 27 failure coefficients such that Equation (7) defines failure when its magnitude exceeds 1. This expression represents the generic mathematical foundation of a failure theory that is influenced by multiple loads (in this case force and moment resultants) and furthermore influenced by the interactions between each when multiple loads are present. The relative influence of each load or interaction is accounted for by the value of each undetermined coefficient C_{ij} or D_i.

Failure coefficients C_{ij} and D_i can be solved given a sufficient amount of known failure points. However, Equation (7) is numerically ill-conditioned given the great disparity in the magnitude of N_{ij} and M_{ij} loads which will cause failure. These values will differ by many orders of magnitude when typical units are utilized (Pa-m and Pa-m^2). This makes accurate solution of failure coefficients impossible when both such load types are present. Thus, Equation (7) must be defined in terms of F_i terms that are normalized with respect to a critical $N_{\max}$ or $M_{\max}$ that would cause failure if it were the only load present.

Coefficients C_{ii} and D_i can be solved by evaluating Equation (7) with a load of F_i and setting all other loads to zero. For example, in order to obtain C_{11} and D_1 a load of $F_1 = N_x$ is applied, all others are set to zero, and Equation (7) reduces to:

$$C_{11}N_x^2 + D_1N_x = 1 \tag{8}$$

Since the DMM has been used to determine the maximum tensile and compressive allowable N_x, each of which must satisfy Equation (8), two independent equations are generated which can be simultaneously solved to yield C_{11} and D_1. Note that, as mentioned earlier, loads have been normalized for numerical robustness (in this case, $N_x/N_{x,\text{critical}}$). The $N_{x,\text{critical}}$ for the plain weave carbon-epoxy in this study was found to be 6.40×10^3 Pa-m; this was used to normalize all force resultant terms. The $M_{x,\text{critical}}$ used to normalize all moment resultant terms was 1.85×10^{-4} Pa-m^2. A complete table of strength values for the carbon-epoxy plain weave textile composite is shown in Table 1. The $\pm$ indicates tension or compression for axial loads but is immaterial for shear or bending loads.

Table 1. Strength values for independent load conditions.

	Strength (+)	Strength (−)
N_x	6.40e3 Pa-m	5.86e3 Pa-m
N_y	6.40e3 Pa-m	5.86e3 Pa-m
N_{xy}	2.11e3 Pa-m	2.11e3 Pa-m
M_x	1.85e-4 Pa-m^2	1.85e-4 Pa-m^2
M_y	1.85e-4 Pa-m^2	1.85e-4 Pa-m^2
M_{xy}	1.06e-4 Pa-m^2	1.06e-4 Pa-m^2

These strength values, modified to the units and notations of classical laminate theory, represent the largest allowable level of each load type when it is the only load present.

Remaining coefficients C_{ij} can be solved by evaluating Equation (7) with the maximum possible $F_i = F_j$ as determined by the DMM results. All other loads are set to zero. This reduction in terms, along with knowledge of previously determined coefficients C_{ii} and D_i, allows for the solution of all remaining coefficients. For example, C_{14} can be determined by applying the maximum possible F_1 and F_4 such that:

$$F_1 = F_4 = \frac{N_x}{N_{\text{critical}}} = \frac{M_x}{M_{\text{critical}}} \tag{9}$$

The failure coefficient is then solved from Equation (7) as:

$$C_{14} = \frac{1}{2F_1F_4}\left(1 - C_{11}F_1^2 - C_{44}F_4^2 - D_1F_1 - D_4F_4\right) \tag{10}$$

The above procedure is similar to that used in deriving Tsai–Wu failure theory for unidirectional composites, e.g., [1]. The results of the above procedures are shown in Tables 2 and 3.

Coefficients D_3 through D_6 are equal to zero since positive and negative failure values are the same for any shear, moment, or twist loads.

For complete evaluation of the 27 failure coefficients, it will generally not be necessary to complete 27 separate physical or simulated experimental evaluations. Exploitation of weave geometry can lead to a significant reduction in the required evaluations. The plain weave under investigation requires 13 evaluations to determine all coefficients, and more complicated weaves will still often exhibit symmetry such that only this amount is required. For the most general, asymmetric textile, 27 evaluations may be required.

Table 2. Normalized failure coefficients C_{ij} for quadratic failure equation. (C_{mn} mth nth).

$n=1$	2	3	4	5	6
$m=1$ 1.02	−0.81	2.45	0.15	0.15	−0.09
2	1.02	2.45	0.15	0.15	−0.09
3		9.29	0.15	0.15	−1.28
4			1.00	−0.65	0.29
5				1.00	0.29
6					3.05

Table 3. Normalized failure coefficients D_i for quadratic failure equation.

D_1	−0.011
D_2	−0.011
D_3	0.000
D_4	0.000
D_5	0.000
D_6	0.000

Twelve evaluations involving a single load F_i both in tension and compression will be needed. Fifteen evaluations will be needed that involve every combination of two loads applied equally (as normalized) until failure. These 27 evaluations may be performed either by physical experiment or simulated via the DMM.

Tables 2 and 3 list failure coefficients for the plain-weave architecture of Figure 1. The same methods shown in this section can easily be applied to any textile architecture of interest. The 27-term quadratic failure equation is robust to adapt to the various forms of failure spaces that may be exhibited by a particular architecture. In this case, a new set of failure coefficients (C_{ij} and D_i) will be determined from the DMM or experimental analysis.

Referring back to Figures 9 and 10, the elliptical curves labeled QFT represent the failure envelopes as predicted by the quadratic stress gradient failure theory of Equation (7), plotted against the DMM failure envelopes. The overall agreement in these diverse failure spaces is seen to be quite suitable, but with regards to Figure 10 it can be seen that there will be 'corners' or portions of the 6D failure space that will be missed with the essentially 6D ellipse space of the quadratic failure theory. Note that the predictions in these cases tend to be conservative in areas of disagreement.

For further comparison and to incorporate more complex loading conditions, several test cases were computed to determine the difference in solutions computed from Equation (7) as compared to the results of the DMM. In general, F_i may be populated by as many as six terms from among (N_x N_y N_{xy} M_x M_y M_{xy}). For cases in which 1, 2, or 3 terms are populated, the solution is accurate to within a few percent. For test cases in which 4, 5, or 6 terms are populated, the average error was seen to be 9.3%, and several example test cases are tabulated below. Care was taken to select a broad spectrum of cases, i.e., both positive and negative values are employed, and multiple load ratios and load types are employed. Load ratios (α) are shown to characterize the range and variety of test cases, and are defined as:

$$\alpha_i = \frac{F_i}{F_1} \tag{11}$$

Further, by maintaining the same load ratios, all predicted failure loads F_i via Equation (7) will maintain a single ratio with respect to DMM failure points. Thus one ratio (as shown in Tables 4–6) can characterize the congruence of these two solutions. For example, a ratio of unity will imply complete agreement between the two solution procedures. A ratio less than 1 indicates a conservative failure prediction, and a ratio greater than 1 implies the converse.

CONCLUSIONS

Based upon failure envelopes constructed by analysis of the microstresses developed in a representative volume element (RVE), two alternate methods for predicting failure envelopes of a plain-weave textile composite have been developed. The previously developed direct micromechanics method (DMM) has been used to construct failure envelopes for a plain weave carbon/epoxy textile composite in plane stress. To allow for the accommodation of stress gradients across the comparatively large geometry of a textile

Table 4. Comparison of quadratic failure equation predictions with DMM results. Test cases below include four populated load terms F_i.

	F_1	F_2	F_3	F_4	F_5	F_6
α	1.00	0.00	0.92	6.67E − 08	0.00	6.67E − 08
DMM	1.20E + 03	0.00E + 00	1.10E + 03	8.00E − 05	0.00E + 00	8.00E − 05
Quadratic theory	1.12E + 03	0.00E + 00	1.02E + 03	7.44E − 05	0.00E + 00	7.44E − 05
Ratio	0.93					
α	1.00	1.83	0.00	6.67E − 08	0.00	6.67E − 08
DMM	1.20E + 03	2.20E + 03	0.00E + 00	8.00E − 05	0.00E + 00	8.00E − 05
Quadratic theory	1.24E + 03	2.27E + 03	0.00E + 00	8.24E − 05	0.00E + 00	8.24E − 05
Ratio	1.03					
α	1.00E + 00	−0.87	0.00	3.91E − 08	−1.40E − 08	0.00
DMM	−2.30E + 03	2.00E + 03	0.00E + 00	−9.00E − 05	3.23E − 05	0.00E + 00
Quadratic theory	−2.55E + 03	2.22E + 03	0.00E + 00	−9.99E − 05	3.59E − 05	0.00E + 00
Ratio	1.11					
α	1.00	0.40	0.00	1.80E − 08	−6.46E − 09	0.00
DMM	−5.00E + 03	−2.00E + 03	0.00E + 00	−9.00E − 05	3.23E − 05	0.00E + 00
Quadratic theory	−5.50E + 03	−2.20E + 03	0.00E + 00	−9.90E − 05	3.55E − 05	0.00E + 00
Ratio	1.1					
α	1.00	−0.50	0.00	−1.61E − 08	−8.08E − 09	0.00
DMM	−4.00E + 03	2.00E + 03	0.00E + 00	6.45E − 05	3.23E − 05	0.00E + 00
Quadratic theory	−3.72E + 03	9.30E + 02	1.53E + 03	6.51E − 05	6.51E − 05	7.44E − 05
Ratio	0.93					

Table 5. Comparison of quadratic failure equation predictions with DMM results. Test cases below include five populated load terms F_i.

	F_1	F_2	F_3	F_4	F_5	F_6
α	1.00	1.00	1.00	6.25E − 08	0.00	6.67E − 08
DMM	1.20E + 03	1.20E + 03	1.20E + 03	7.50E − 05	0.00E + 00	8.00E − 05
Quadratic theory	1.04E + 03	1.04E + 03	1.04E + 03	6.53E − 05	0.00E + 00	6.96E − 05
Ratio	0.87					
α	1.00	1.67	1.20	4.67E − 08	5.33E − 08	0.00
DMM	1.50E + 03	2.50E + 03	1.80E + 03	7.00E − 05	8.00E − 05	0.00E + 00
Quadratic theory	1.32E + 03	2.20E + 03	1.58E + 03	6.16E − 05	7.04E − 05	0.00E + 00
Ratio	0.88					
α	1.00	−1.33	−1.07	−4.67E − 08	3.33E − 08	0.00
DMM	−1.50E + 03	2.00E + 03	1.60E + 03	7.00E − 05	−5.00E − 05	0.00E + 00
Quadratic theory	−1.32E + 03	1.76E + 03	1.41E + 03	6.16E − 05	−4.40E − 05	0.00E + 00
Ratio	0.88					
α	1.00	1.33	1.00	−3.33E − 08	2.67E − 08	0.00
DMM	−1.50E + 03	−2.00E + 03	−1.50E + 03	5.00E − 05	−4.00E − 05	0.00E + 00
Quadratic theory	−1.32E + 03	−1.76E + 03	−1.32E + 03	4.40E − 05	−3.52E − 05	0.00E + 00
Ratio	0.88					
α	1.00	−0.45	0.45	2.27E − 08	0.00	3.18E − 08
DMM	−2.20E + 03	1.00E + 03	−1.00E + 03	−5.00E − 05	0.00E + 00	−7.00E − 05
Quadratic theory	−2.16E + 03	9.80E + 02	−9.80E + 02	−4.90E − 05	0.00E + 00	−6.86E − 05
Ratio	0.98					

Table 6. Comparison of quadratic failure equation predictions with DMM results. Test cases below include fully populated load terms F_i.

	F_1	F_2	F_3	F_4	F_5	F_6
α	1.00	0.56	0.92	3.89E − 08	3.89E − 08	4.44E − 08
DMM	1.80E + 03	1.00E + 03	1.65E + 03	7.00E − 05	7.00E − 05	8.00E − 05
Quadratic theory	1.55E + 03	8.60E + 02	1.42E + 03	6.02E − 05	6.02E − 05	6.88E − 05
Ratio	0.86					
α	1.00	1.00	0.52	1.33E − 08	1.33E − 08	1.33E − 08
DMM	3.00E + 03	3.00E + 03	1.55E + 03	4.00E − 05	4.00E − 05	4.00E − 05
Quadratic theory	2.61E + 03	2.61E + 03	1.35E + 03	3.48E − 05	3.48E − 05	3.48E − 05
Ratio	0.87					
α	1.00	−0.73	−0.33	−1.33E − 08	1.33E − 08	1.33E − 08
DMM	−3.00E + 03	2.20E + 03	1.00E + 03	4.00E − 05	−4.00E − 05	−4.00E − 05
Quadratic theory	−2.85E + 03	2.09E + 03	9.50E + 02	3.80E − 05	−3.80E − 05	−3.80E − 05
Ratio	0.95					
α	1.00	−0.67	0.67	−2.67E − 08	5.33E − 08	−3.33E − 08
DMM	−1.50E + 03	1.00E + 03	−1.00E + 03	4.00E − 05	−8.00E − 05	5.00E − 05
Quadratic theory	−1.44E + 03	9.60E + 02	−9.60E + 02	3.84E − 05	−7.68E − 05	4.80E − 05
Ratio	0.96					
α	1.00	0.59	0.88	3.53E − 08	3.53E − 08	4.71E − 08
DMM	−1.70E + 03	−1.00E + 03	−1.50E + 03	−6.00E − 05	−6.00E − 05	−8.00E − 05
Quadratic theory	−1.45E + 03	−8.50E + 02	−1.28E + 03	−5.10E − 05	−5.10E − 05	−6.80E − 05
Ratio	0.85					

RVE, micromechanical analysis had been performed in terms of classical laminate theory force and moment resultants [*N*], [*M*]. A parametric ellipse-fitting scheme which accurately predicts trends in failure envelopes for a given 3D failure space has been developed by analysis of failure ellipse parameters. This method for predicting failure envelopes was found to agree with DMM results to within a few percent. A second method involves development of a 27-term quadratic stress gradient failure criterion to predict failure under 6D loading conditions. The quadratic failure criterion was found to agree with DMM results within an average deviation of 9.3%, but the method is more robust in terms of its ability to predict failure from more complex loading cases.

NOMENCLATURE

ε^M = macroscopic level strain
κ^M = macroscopic level curvature
σ^e = element level stress
a = RVE width
b = RVE depth
N_i = force resultant in the i direction
N_{xy} = shear force resultant in the x–y plane
M_i = moment resultant in the i direction
M_{xy} = torque resultant in the x–y plane

ε_i = normal strain in the i direction
γ_{xy} = shear strain in the x–y plane
κ_i = curvature in the i direction
κ_{xy} = twist in the x–y direction
$[A]$ = in-plane stiffness matrix
$[B]$ = strain-curvature coupling matrix
$[D]$ = flexural stiffness matrix
z = distance from RVE midplane in the height direction
θ = ellipse major axis orientation angle
u_0 = ellipse center point coordinate, abscissa
v_0 = ellipse center point coordinate, ordinate
a = ellipse major axis length
b = ellipse minor axis length
C_{ij} = failure coefficient
F_i = load, in terms of force or moment resultant
D_i = failure coefficient
α = load ratio

ACKNOWLEDGEMENT

This work was performed under Army Research Office contract DAAD19-02-1-0330 with Dr. Bruce LaMattina as the Grant Monitor. This support is gratefully acknowledged.

REFERENCES

1. Tsai, S.W. and Hahn, H.T. (1980). *Introduction to Composite Materials*, Technomic Publishing Co, Lancaster, PA.
2. Karkkainen, R.L. and Sankar, B.V. (2006). A Direct Micromechanics Method for Analysis of Failure Initiation of Plain Weave Textile Composites, *Journal of Composites Science and Technology*, **66**: 137–150.
3. Whitcomb, J.K. and Srirengan, K. (1996). Effect of Various Approximations on Predicted Progressive Failure in Plain Weave Composites, *Composite Structures*, **34**: 13–20.
4. Woo, K. and Whitcomb, J.D. (2000). A Post Processor Approach for Stress Analysis of Woven Textile Composites, *Composites Science and Technology*, **60**: 693–704.
5. Tang, X. and Whitcomb, J.D. (2003). General Techniques for Exploiting Periodicity and Symmetries in Micromechanics Analysis of Textile Composites, *Journal of Composite Materials*, **37**: 13.
6. Whitcomb, J.D., Chapman, C.D. and Srirengan, K. (1998). Analysis of Plain-Weave Composites Subjected to Flexure, *Mechanics of Composite Materials and Structures*, **5**: 41–53.
7. Cox, B.N. and Dadkhah, M.S. (1994). A Binary Model of Textile Composites: I-Formulation, *Acta Metallurgica et Materiala*, **42**(10): 3463.
8. Yang, Q. and Cox, B.N. (2003). Predicting Local Strains in Textile Composites Using the Binary Model Formulation, In: *Proceedings of the ICCM 2003*, San Diego, CA, July.
9. Bogdanovich, A.E. and Pastore, C.M. (1996). Material-Smart Analysis of Textile-Reinforced Structures, *Composites Science and Technology*, **56**: 291–309.
10. Bogdanovich, A.E. (2003). Multiscale Predictive Analysis of 3-D Woven Composites, In: *SAMPE 35th International Technical Conference*, CD ROM Proceedings, Dayton, OH, September.

2

11. Quek, S.C. et al. (2004). Compressive Response and Failure of Braided Textile Composites: Part 2, Computations, *International Journal of Nonlinear Mechanics*, **39**: 649–663.
12. Quek, S.C. et al. (2004). Compressive Response and Failure of Braided Textile Composites: Part 1, Experiments, *International Journal of Nonlinear Mechanics*, **39**: 635–648.
13. Gosse J.H. and Christensen, S. (2001). Strain Invariant Failure Criteria for Polymers in Composite Materials, *AIAA-2001-1184*.
14. Tay, T.E., Tan, V.B.C. and Tan, S.H.N. (2005). Element-failure: An Alternative to Material Property Degradation Method for Progressive Damage in Composite Structures, *Journal of Composite Materials*, **39**(18) : 1659–1675.
15. Zhu, H., Sankar, B.V. and Marrey, R.V. (1998). Evaluation of Failure Criteria for Fiber Composites Using Finite Element Micromechanics, *Journal of Composite Materials*, **32**(8): 766–782.
16. Marrey, R.V. and Sankar, B.V. (1995). Micromechanical Models for Textile Structural Composites, *NASA CR-198229*.
17. Sankar, B.V. and Marrey, R.V. (1997). Analytical Method for Micromechanics of Textile Composites, *Composites Science and Technology*, **57**(6): 703–713.
18. Marrey, R.V. and Sankar, B.V. (1997). A Micromechanical Model for Textile Composite Plates, *J. of Composite Materials*, **31**(12): 1187–1213.
19. Carvelli, V. and Poggi, C. (2001). A Homogenization Procedure for the Numerical Analysis of Woven Fabric Composites, *Composites Part A: Applied Science and Manufacturing*, **32**: 1425–1432.